

Stability Analysis of Ultrasound Thick-Shell Contrast Agents

Xiaozhen Lu^{*}, Georges L. Chahine[†], and Chao-Tsung Hsiao^{*},

DYNAFLOW, INC.

10621-J Iron Bridge Road

Jessup, Maryland 20794

www.dynafLOW-inc.com

^{**} Research Scientist, DYNAFLOW, INC., Email: xiaozhen@dynafLOW-inc.com

[†] President, DYNAFLOW, INC., Email: glchahine@dynafLOW-inc.com

^{*} Principal Research Scientist, DYNAFLOW, INC., Email: ctsung@dynafLOW-inc.com

Abstract

The stability of thick shell encapsulated bubbles is studied analytically. 3-D small perturbations are introduced to the spherical oscillations of a contrast agent bubble in response to a sinusoidal acoustic field with different amplitudes of excitation. The equations of the perturbation amplitudes are derived using asymptotic expansions and linear stability analysis is then applied to the resulting differential equations. The stability of the encapsulated microbubbles to nonspherical small perturbations is examined by solving an eigenvalue problem. The approach then identifies the fastest growing perturbations which could lead to the breakup of the encapsulated microbubble or contrast agent.

1. INTRODUCTION

Ultrasound contrast agents are encapsulated microbubbles which are usually formed with a high molecular weight gas core and a shell.¹⁻³ A wide variety of materials have been used for the shell material such as oils, lipids, rigid polymers, and albumins. Ultrasound contrast agents were originally developed to enhance diagnostic imaging and have recently been incorporated into therapeutic applications.

By resonating in an ultrasound beam, microbubbles are much more reflective than normal body tissues, thus they enhance the signals from a Doppler examination. Depending on the intensity of the transmitted ultrasound beam, bubbles behavior differently.⁴ At low intensity, the bubbles act as simple but powerful enhancers. At slightly higher intensity, the bubbles emit harmonics as they undergo non-linear oscillations. At even higher intensity, the bubbles are disrupted, emitting a strong transient echo. Understanding the behavior of the bubbles is important to get optimal imaging parameters and to reduce bioeffects such as hemolysis⁵⁻⁷ and hemorrhage.⁸

The capability of delivering drug to the targeted area makes therapeutic ultrasound contrast agents attractive to chemotherapy drug development because many chemotherapy drugs are toxic to normal tissues. For therapeutic ultrasound contrast agents, the drug is suspended within a highly viscous thick liquid shell,⁹ which stabilizes the encapsulated bubble and keeps it inert until the contrast agent reaches a specific target. With an appropriate acoustic amplitude and frequency, the encapsulated microbubble is excited and breaks up releasing the drugs when it is fragmented. A proper selection of shell material and thickness and an appropriate use of ultrasound would render the contrast agents powerful targeted drug delivery vehicles. Characterization and understanding of the fragmentation mechanism of a contrast agent is pivotal to its use for drug delivery.

The ultrasonic fragmentation threshold for an encapsulated microbubble depends on the microbubble size, shell thickness, and shell and gas properties.^{10,11} Using a high intensity source and a large number of cycles would disrupt all types and sizes of contrast agent, but cannot be always applied safely in a clinical environment. Understanding of the forces involved in the breakup of a particular type of agent is therefore paramount to avoiding expensive and lengthy trial and error experiments, and to minimizing risk to patients. Presently however, the dynamic mechanisms involved in shell breakup are not well understood.

The application of contrast agent to vectored drug delivery requires controlled fragmentation of microbubbles. The onset of bubble breakup is directly linked to the loss of spherical symmetry due to growing instabilities at the interface between two of the involved fluids: gas, viscous shell content, and host liquid. For an air bubble, stability of the spherical the shape has been theoretically studied some time back using linear stability analysis.^{1,12} For an encapsulated bubble, stability analysis is more complicated due to the presence of the thick shell layer. While several experimental studies have been conducted concerning the fragmentation of the contrast agent,¹³ less work has been published on theoretical modeling. The present study will address the shape stability of an encapsulated bubble with finite thickness subject to irrotational perturbations using linear stability analysis.

2. FORMULATION OF THE PROBLEM

We consider a single spherical bubble encapsulated in a thick shell of a viscous liquid. We define, as shown in Figure 1, the dimensional[‡] inner and outer radius of the bubble shell as R_1^* and R_2^* respectively. The densities and viscosities in the viscous shell (*inner domain*) are ρ_1^*

[‡] We will use stars for the dimensional quantities, to distinguish from non-starred characters for normalized quantities. This will simplify the presentation later.

and μ_1^* , and in the surrounding host liquid (*outer domain*) they are ρ_2^* and μ_2^* . Both liquids in the inner and outer domain are assumed incompressible, while the gas inside the bubble is compressible. The surface tension coefficients between each two fluids at the interfaces 1 and 2 are γ_1^* and γ_2^* at R_1^* and R_2^* respectively.

In this study the wavelength of the imposed acoustic field in the gaseous bubble core is two orders of magnitude larger than the bubble radius and in this perturbation study the resulting velocities in the gas are very small compared to the sound speed. Therefore, the pressure, p_g^* , inside the gas core is assumed to be uniform and to follow a polytropic compression law. The inner domain pressures at the two interfaces at $r^* = R_1^*$ and $r^* = R_2^*$ are p_1^* and p_2^* respectively. The outer domain pressure at Interface 2 at $r^* = R_2^*$ is p_3^* . The imposed pressure far from the bubble is $P_\infty(t)$.

To non-dimensionalize the problem, we use the initial outer radius R_{20}^* as the length scale and T^* as the time scale. (T^* could be selected as the characteristic period of the acoustic field driving pressure of amplitude P_a and period $1/f$), and the outer domain liquid density, ρ_2^* , as the density scale. Then the velocity scale is

$$U^* = \frac{R_{20}^*}{T^*}. \quad (1)$$

The non-dimensional radial coordinates and times can then be defined as:

$$r = \frac{r^*}{R_{20}^*}, \quad t = \frac{T^*}{T^*}, \quad (2)$$

and the non-dimensional inner and outer radii are

$$R_1 = \frac{R_1^*}{R_{20}^*}, \quad R_2 = \frac{R_2^*}{R_{20}^*}, \quad (3)$$

The non-dimensional densities are

$$\rho_1 = \frac{\rho_1^*}{\rho_2^*}, \quad \rho_2 = 1, \quad (4)$$

and the non-dimensional pressures are

$$p = \frac{p^*}{\rho_2^* U^{*2}}, \quad p_g = \frac{p_g^*}{\rho_2^* U^{*2}}, \quad P_\infty = \frac{P_\infty^*}{\rho_2^* U^{*2}}. \quad (5)$$

We will use these non-dimensional quantities below unless specified.

Both inner and outer domain liquids will be considered viscous and will be solved using the continuity and momentum conservation equations.

3. DYNAMICS EQUATION OF A THICK-SHELLED SPHERICAL MICROBUBBLE

Conservation of mass and incompressibility in the outer domain are easy to express due to the spherical symmetry of the problem and lead to the following expression for the radial velocity, u_{2r} , in the host liquid:

$$u_{2r} = \frac{\dot{R}_2 R_2^2}{r^2}. \quad (6)$$

The same applies to the inner problem, i.e. to the thick shell medium, to give:

$$u_{1r} = \frac{\dot{R}_1 R_1^2}{r^2}. \quad (7)$$

Equality of the velocities at the interface between the shell and the host liquid,

$$u_{2r}(R_2) = u_{1r}(R_2), \quad (8)$$

leads to:

$$\dot{R}_2 = \dot{R}_1 \frac{R_1^2}{R_2^2}. \quad (9)$$

The momentum equations applied to the inner and outer domain are:

$$\rho_1 \left(\frac{\partial u_r}{\partial t} + u_r \frac{\partial u_r}{\partial r} \right) = \frac{1}{R_{e1}} \frac{\partial}{\partial r} \left(\frac{1}{r^2} \frac{\partial}{\partial r} (r^2 u_r) \right) - \frac{\partial p}{\partial r}, \quad (10)$$

$$\rho_2 \left(\frac{\partial u_r}{\partial t} + u_r \frac{\partial u_r}{\partial r} \right) = \frac{1}{R_{e2}} \frac{\partial}{\partial r} \left(\frac{1}{r^2} \frac{\partial}{\partial r} (r^2 u_r) \right) - \frac{\partial p}{\partial r}, \quad (11)$$

with

$$R_{e1} = \rho_2^* U^* R_{20}^* / \mu_1, \quad R_{e2} = \rho_2^* U^* R_{20}^* / \mu_2 \quad (12)$$

where R_{e1} and R_{e2} are the inner and outer domains Reynolds numbers. Substituting (7) into (10)

and (6) into (11) and integrating equation (10) from $R_1 \rightarrow R_2$ and equation (11) from $R_2 \rightarrow \infty$,

we obtain:

$$\rho_1 \left(R_2 \ddot{R}_2 + \frac{3}{2} \dot{R}_2^2 \right) - p_2 = \rho_1 \left(R_1 \ddot{R}_1 + \frac{3}{2} \dot{R}_1^2 \right) - p_1, \quad (13)$$

$$\rho_2 \left(R_2 \ddot{R}_2 + \frac{3}{2} \dot{R}_2^2 \right) = p_3 - P_\infty, \quad (14)$$

where P_∞ is the imposed acoustic pressure, and the double dots denote the second order time

derivative $\frac{d^2}{dt^2}$. The normal stress balance on the inner and outer interfaces gives:

$$p_1 = p_v + p_g - \frac{1}{W_{e1}} \mathbf{C}_1 + \frac{1}{R_{e1}} \mathbf{n} \cdot (\nabla \mathbf{u} + \nabla \mathbf{u}^T) \cdot \mathbf{n} \Big|_{r=R_1}, \quad (15)$$

$$p_3 - p_2 = -\frac{1}{W_{e2}} \mathbf{C}_2 + \left(\frac{1}{R_{e2}} - \frac{1}{R_{e1}} \right) \mathbf{n} \cdot (\nabla \mathbf{u} + \nabla \mathbf{u}^T) \cdot \mathbf{n} \Big|_{r=R_2}, \quad (16)$$

where the weber numbers W_{e1} and W_{e2} are defined as:

$$W_{e1} = \rho_2^* U^2 R_{20} / \gamma_1, \quad W_{e2} = \rho_2^* U^2 R_{20} / \gamma_2. \quad (17)$$

\mathbf{n} is the unit vector normal to the inner or outer surface, and

$$\mathbf{C}_i = \nabla \cdot \mathbf{n}_i, \quad (i = 1, 2) \quad (18)$$

are the curvatures of the inner or outer surface.

Using (6) and (7) equations (15) and (16) become:

$$p_1 = p_v + p_g - \frac{2}{W_{e1} R_1} - \frac{4}{R_{e1}} \frac{R_1 \dot{R}_1}{R_1}, \quad (19)$$

$$p_3 = p_2 - \frac{2}{W_{e1} R_2} - 4 \left(\frac{1}{R_{e2}} - \frac{1}{R_{e1}} \right) \frac{\dot{R}_2}{R_2}. \quad (20)$$

Substituting (19) and (20) into (13) and (14) p_2 can be cancelled and we obtain

$$\begin{aligned} & R_2 \ddot{R}_2 \left((1 - \rho_1) + \rho_1 \frac{R_2}{R_1} \right) + (1 - \rho_1) \frac{3}{2} \dot{R}_2^2 + \rho_1 \dot{R}_2^2 \left(2R_2 / R_1 - \frac{1}{2} (R_2 / R_1)^4 \right) \\ & = p_v + p_g - P_\infty - \left(\frac{2}{W_{e1} R_1} + \frac{2}{W_{e2} R_2} \right) - 4 \frac{1}{R_{e2}} \frac{\dot{R}_2}{R_2} - 4 \frac{1}{R_{e1}} \frac{\dot{R}_2}{R_2} \left(\left(\frac{R_2}{R_1} \right)^3 - 1 \right). \end{aligned} \quad (21)$$

A similar differential equation is obtained for R1, using Equation (9).

When the liquid inside the shell layer is the same as the host liquid, i.e. when the $\rho_1 = 1$, $R_{e1} = R_{e2}$ and $1/W_{e2} = 0$, the above equation (21) reduces to the conventional Rayleigh-Plesset equation.

4. HARMONIC PERTURBATIONS OF THE SPHERICAL SOLUTION

Equation (21) describes the spherical oscillations of the shelled bubble. To investigate how stable this spherical motion is, 3-D small perturbations can be introduced to the solution and

the stability can be determined by investigating whether these perturbations grow with time or not. We consider such perturbations below.

4.1 Flow Solution in the Host Liquid

Let us consider harmonic nonspherical small perturbations of the outer microbubble such that the nondimensional equation of the surface is modified from $r = R_2(t)$ to

$$S_2 = r - R_2(t) - \varepsilon b_n Y_n^m = 0, \quad b_n = O(1), \quad \varepsilon \ll 1, \quad (22)$$

where Y_n^m are spherical harmonic functions and $n \neq 0$.

The microbubble volume is unchanged after the perturbation because:

$$\begin{aligned} V &= \int_0^{2\pi} \int_0^\pi \int_0^{R_2 + \varepsilon b_n Y_n^m} r^2 dr \sin \theta d\theta d\varphi \\ &= \frac{1}{3} \int_0^{2\pi} \int_0^\pi (R_2 + \varepsilon b_n P_n^m e^{im\varphi})^3 \sin \theta d\theta d\varphi \\ &= \frac{1}{3} \int_0^{2\pi} \int_0^\pi (R_2^3 + 3R_2^2 \varepsilon b_n P_n^m e^{im\varphi}) \sin \theta d\theta d\varphi + O(\varepsilon^2) \\ &= \frac{4\pi R_2^3}{3} - 3R_2^2 \varepsilon b_n \int_0^{2\pi} e^{im\varphi} d\varphi \int_0^\pi P_n^m(\cos \theta) d(\cos \theta) + O(\varepsilon^2), \end{aligned} \quad (23)$$

where $P_n^m(\cos \theta)$ are Legendre polynomials. For $n \neq 0$, the orthogonality of the Legendre polynomials gives:

$$\int_0^\pi P_n^m(\cos \theta) d(\cos \theta) = 0. \quad (24)$$

Thus, up to order ε , the contribution of the perturbation to the microbubbles volume, (23), is zero.

To investigate the stability of the oscillations, one needs to investigate whether the added perturbations will grow or decay over time. Figure 2 illustrates the shapes that will result from instability of the various small perturbation modes. *These illustrate only for visualization, the shapes long after asymptotic expansions are no longer valid.* With mode $n=1$, a jet can be

formed if instability develops, with mode $n=2$, the bubble surface becomes ellipsoidal and when the perturbation grows, the bubble tends to split into two smaller bubbles. With modes $n=3$ or 4, the perturbations could result in break up of the bubble into 3 or 4 smaller bubbles.

The corresponding perturbed velocity potential in the outer domain can be written as:

$$\Phi_2 = \phi_2 + \varepsilon \phi_2', \quad (25)$$

where ϕ_2 is the unperturbed spherical velocity potential, and ϕ_2' is the nonspherical small perturbation of this velocity potential. Both are potential and satisfy the Laplace equation. The harmonic expansion of ϕ_2' can be obtained by considering the kinematic boundary condition at the interface between the shell and the host liquid. This can be written:

$$\frac{dS_2}{dt} = \frac{\partial S_2}{\partial t} + \mathbf{U} \cdot \nabla S_2|_{S_2=0} = 0, \quad \text{with} \quad \mathbf{U} = \nabla \Phi_2. \quad (26)$$

$$\text{Using (22) and (25), we have: } \frac{\partial S_2}{\partial t} = -R_2 - \varepsilon \dot{b}_n Y_n^m, \quad (27)$$

$$\nabla S_2|_{S_2=0} = \begin{pmatrix} 1 \\ -\varepsilon \frac{b_n}{R_2} \partial_\theta Y_n^m \\ -\varepsilon \frac{b_n}{R_2 \sin \theta} \partial_\varphi Y_n^m \end{pmatrix} + O(\varepsilon^2) \quad (28)$$

and

$$\mathbf{U}|_{S_2=0} = \begin{pmatrix} \frac{\partial \phi_2}{\partial r} + \varepsilon \left(\frac{\partial \phi_2'}{\partial r} + \frac{\partial^2 \phi_2}{\partial r^2} b_n Y_n^m \right) \\ \frac{\varepsilon}{R_2} \frac{\partial \phi_2'}{\partial \theta} \\ \frac{\varepsilon}{R_2 \sin \theta} \frac{\partial \phi_2'}{\partial \varphi} \end{pmatrix} \Bigg|_{r=R_2} + O(\varepsilon^2), \quad (29)$$

Substituting in equation (26) we obtain:

$$\left(-\dot{R}_2 + \frac{\partial \phi_2}{\partial r} \right) \Big|_{r=R_2} + \varepsilon \left(-\dot{b}_n Y_n^m + \frac{\partial \phi_2'}{\partial r} + \frac{\partial^2 \phi_2}{\partial r^2} b_n Y_n^m \right) \Big|_{r=R_2} + O(\varepsilon^2) = 0 \quad . \quad (30)$$

Separating the ε order, we have

$$\left(-\dot{R}_2 + \frac{\partial \phi_2}{\partial r} \right) \Big|_{R_2} = 0, \quad (31)$$

$$\left(-\dot{b}_n Y_n^m + \frac{\partial \phi_2'}{\partial r} + \frac{\partial^2 \phi_2}{\partial r^2} b_n Y_n^m \right) \Big|_{r=R_2} = 0. \quad (32)$$

The far field boundary conditions can also be written

$$r \rightarrow \infty, \quad \phi_2 = 0, \quad \phi_2' = 0. \quad (33)$$

The solution of the above equations (31) and (32) with boundary conditions (33) lead to the following spherical and perturbed velocity potential of the outer domain:

$$\Phi_2 = -\frac{R_2^2 \dot{R}_2}{r} - \varepsilon \left(2b_n \dot{R}_2 + \dot{b}_n R_2 \right) \left(\frac{R_2}{r} \right)^{n+1} \frac{Y_n^m}{n+1} \quad . \quad (34)$$

4.2 Flow Solution in the Microbubble Shell

In the microbubble shell the velocity potential is Φ_1 , and the kinematical condition on the interface shell – host liquid can be written as in (26):

$$\frac{\partial S_1}{\partial t} + \mathbf{U} \cdot \nabla S_1 \Big|_{S_1=0} = 0 \quad \text{with} \quad \mathbf{U} = \nabla \Phi_1, \quad (35)$$

and

$$\Phi_1 \Big|_{S_2=0} = \Phi_2 \Big|_{S_2=0}. \quad (36)$$

Using the same technique as in the previous section for Φ_2 , we obtain the solution of Φ_1 :

$$\Phi_1 = -\frac{R_2^2 \dot{R}_2}{r} - \varepsilon \left(2b_n \dot{R}_2 + \dot{b}_n R_2 \right) \left(\frac{R_2}{r} \right)^{n+1} \frac{Y_n^m}{n+1}. \quad (37)$$

The microbubble gaseous surface equation can be written as:

$$S_1 = r - R_1(t) - \varepsilon a_l Y_l^k = 0, \quad a_l = O(1) \quad \varepsilon \ll 1, \quad (38)$$

on which the following kinematic boundary condition applies:

$$\frac{\partial S_1}{\partial t} + \nabla \Phi_1 \cdot \nabla S_1 \Big|_{S_1=0} = 0. \quad (39)$$

By substituting equation (37) to (39) and separating the order of each term, we *obtain*:

$$\left(2b_n \dot{R}_2 + \dot{b}_n R_2 \right) (R_2)^{n+1} Y_n^m = \left(2a_l \dot{R}_1 + \dot{a}_l R_1 \right) (R_1)^{n+1} Y_l^k. \quad (40)$$

Due to the orthogonality of the harmonic functions, for equation (40) to be true, we need when $n=l$ and $m=k$:

$$\left(2b_n \dot{R}_2 + \dot{b}_n R_2 \right) (R_2)^{n+1} = \left(2a_n \dot{R}_1 + \dot{a}_n R_1 \right) (R_1)^{n+1}, \quad (41)$$

And when $n \neq l$ or $m \neq k$, then we have:

$$\begin{aligned} 2b_n \dot{R}_2 + \dot{b}_n R_2 = 0; \quad i.e. \quad \frac{d}{dt} (b_n R_2^2) = 0, \\ 2a_l \dot{R}_1 + \dot{a}_l R_1 = 0; \quad i.e. \quad \frac{d}{dt} (a_l R_1^2) = 0. \end{aligned} \quad (42)$$

If R_1 and R_2 are periodic solutions, so are a_l and b_n , then the perturbations do not grow or decay over the cycles. This kind of perturbation mode does not affect the stability of the oscillations. Therefore, we will consider the perturbations of the form $n=l$ and $m=k$ only, and from equations (42), we can rewrite equation (37) as:

$$\Phi_1 = -\frac{R_1^2 \dot{R}_1}{r} - \frac{\varepsilon}{n+1} \left(2a_n \dot{R}_1 + \dot{a}_n R_1 \right) \left(\frac{R_1}{r} \right)^{n+1} Y_n^m. \quad (43)$$

4.3 Equations for the oscillations

Application of the Bernoulli equation in the inner and outer domain between interfaces 1 and 2 and then interface 2 and infinity gives:

$$\begin{aligned} \left[\frac{\partial \Phi_1}{\partial t} + \frac{1}{2} (\nabla \Phi_1)^2 + \frac{P_2}{\rho_1} \right]_{S_2=0} &= \left[\frac{\partial \Phi_1}{\partial t} + \frac{1}{2} (\nabla \Phi_1)^2 + \frac{P_1}{\rho_1} \right]_{S_1=0}, \\ \left[\frac{\partial \Phi_2}{\partial t} + \frac{1}{2} (\nabla \Phi_2)^2 + \frac{P_3}{\rho_2} \right]_{S_2=0} &= \frac{P_\infty}{\rho_2}. \end{aligned} \quad (44)$$

Also, application of the normal stress balances on the inner and outer shell surfaces gives:

$$\begin{aligned} P_1 &= p_v + P_g - \frac{1}{W_{e1}} \mathbf{C}_1 + \frac{1}{R_{e1}} \mathbf{n} \cdot (\nabla \mathbf{U} + \nabla \mathbf{U}^T) \cdot \mathbf{n} \Big|_{S_1=0}, \\ P_3 - P_2 &= -\frac{1}{W_{e2}} \mathbf{C}_2 + \left(\frac{1}{R_{e2}} - \frac{1}{R_{e1}} \right) \mathbf{n} \cdot (\nabla \mathbf{U} + \nabla \mathbf{U}^T) \cdot \mathbf{n} \Big|_{S_2=0}. \end{aligned} \quad (45)$$

Upon substitution using equation (34) and (43) into equations(44) and (45), canceling P_1 , P_2 and P_3 , and separating the orders in ε , we re-obtain equation (21) and

$$\begin{aligned} &\left((\rho_2 - \rho_1) \left(\frac{R_1}{R_2} \right)^{n+1} + \rho_1 \right) \ddot{a}_n = - \left(3 \frac{\dot{R}_1}{R_1} \rho_1 + \frac{2(n+2)(2n+1)}{R_{e1} R_1^2} \right) \dot{a}_n \\ &+ \left((n-1) \frac{\ddot{R}_1}{R_1} \rho_1 - \frac{1}{W_{e1}} \frac{(n-1)(n+1)(n+2)}{R_1^3} - \frac{4(n-1)(n+1)\dot{R}_1}{R_{e1} R_1^3} \right) a_n \\ &- (\rho_2 - \rho_1) \left(\frac{3\dot{a}_n \dot{R}_1 + 2a_n \ddot{R}_1}{R_1} \left(\frac{R_1}{R_2} \right)^{n+1} + (n+1) \frac{2a_n \dot{R}_1 + \dot{a}_n R_1}{R_1^2} \left(\frac{R_1}{R_2} \right)^{n+1} \dot{R}_1 \left(1 - \left(\frac{R_1}{R_2} \right)^3 \right) - \frac{3\dot{b}_n \dot{R}_2 + 2b_n \ddot{R}_2}{R_1} \right) \\ &- \left(\frac{3(\rho_2 - \rho_1)\dot{R}_2}{R_1} + \left(\frac{1}{R_{e2}} - \frac{1}{R_{e1}} \right) \frac{2(n+1)(n+2)}{R_1 R_2} \right) \dot{b}_n \\ &+ \left(\frac{(n-1)(\rho_2 - \rho_1)\ddot{R}_2}{R_1} - \frac{1}{W_{e2}} \frac{(n-1)(n+1)(n+2)}{R_1 R_2^2} - \left(\frac{1}{R_{e2}} - \frac{1}{R_{e1}} \right) \frac{4(n-1)(n+1)\dot{R}_2}{R_1 R_2^2} \right) b_n. \end{aligned} \quad (46)$$

and

$$\dot{b}_n = \frac{2a_n \dot{R}_1 + \dot{a}_n R_1 \left(\frac{R_1}{R_2}\right)^{n+2}}{R_1} - 2b_n \frac{\dot{R}_2}{R_2}. \quad (47)$$

The natural frequency of this system can be shown to be:

$$\omega_n^2 = \frac{1}{W_{e1}} \frac{(n-1)(n+1)(n+2)}{R_1^3} \left[1 + \frac{W_{e1}}{W_{e2}} \left(\frac{R_1}{R_2}\right)^{n+4} \right] \left[(\rho_2 - \rho_1) \left(\frac{R_1}{R_2}\right)^{n+1} + \rho_1 \right]^{-1}, \quad (48)$$

which includes viscosity and surface tension effects. It is trivial to verify that by setting $\rho_2 = \rho_1$ and removing the outer surface, eq. (46) recovers the well-known single bubble shape oscillation equation.

$$\ddot{a}_n = - \left(3 \frac{\dot{R}_1}{R_1} + \frac{2(n+1)(n+2)}{R_{e1} R_1^2} \right) \dot{a}_n + (n-1) \left(\frac{\ddot{R}_1}{R_1} - \frac{1}{W_{e1}} \frac{(n+1)(n+2)}{R_1^3} - \frac{4(n+1)\dot{R}_1}{R_{e1} R_1^3} \right) a_n, \quad (49)$$

which has as natural frequency:

$$\omega_n^2 = \frac{1}{W_{e1}} \frac{(n-1)(n+1)(n+2)}{R_1^3}. \quad (50)$$

4.4 EIGENVALUE PROBLEM

After the spherical oscillations according to equation (21) reach a steady periodic state, the coefficients in equations (46), (47) are periodic functions of time and, therefore, Floquet theory applies,¹⁴ according to which the solution at the end of a cycle $(a_n, \dot{a}_n, b_n)_{t=t_0+1}$ is linearly related to the value at the beginning of a cycle $(a_n, \dot{a}_n, b_n)_{t=t_0}$.

Let's define

$$\mathbf{X}(t) = \begin{pmatrix} a_n \\ \dot{a}_n \\ b_n \end{pmatrix}. \quad (51)$$

To determine the stability of the oscillations, we need to find the value of λ such that

$$\mathbf{X}(t_0 + 1) = \lambda \mathbf{X}(t_0) \quad (52)$$

for non-zero $\mathbf{X}(t_0)$. If $|\lambda| > 1$, the oscillations will grow in time and are unstable, otherwise the oscillations are stable. Suppose we have

$$\mathbf{X}(t_0) = \begin{pmatrix} \alpha_1 \\ \alpha_2 \\ \alpha_3 \end{pmatrix}, \quad (53)$$

where $\alpha_1, \alpha_2, \alpha_3$ are constants, and let us introduce a set of orthogonal 3-D base vectors

$\mathbf{V}^i (i=1,2,3),:$

$$\mathbf{V}^1(t_0) = \begin{pmatrix} 1 \\ 0 \\ 0 \end{pmatrix}, \quad \mathbf{V}^2(t_0) = \begin{pmatrix} 0 \\ 1 \\ 0 \end{pmatrix}, \quad \mathbf{V}^3(t_0) = \begin{pmatrix} 0 \\ 0 \\ 1 \end{pmatrix}, \quad (54)$$

then

$$\mathbf{X}(t_0) = \sum_{i=1}^3 \alpha_i \mathbf{V}^i(t_0). \quad (55)$$

Since $\mathbf{X}(t_0 + 1)$ is linearly related to $\mathbf{X}(t_0)$, we have

$$\mathbf{X}(t_0 + 1) = \sum_{i=1}^3 \alpha_i \mathbf{V}^i(t_0 + 1), \quad (56)$$

where $\mathbf{V}^i(t_0 + 1) (i=1,2,3)$, is the value of $\begin{pmatrix} a_n \\ \dot{a}_n \\ b_n \end{pmatrix} \Big|_{t=t_0+1}$ with the initial condition being $\mathbf{V}^i(t_0)$.

Equation (52) becomes:

$$\sum_{i=1}^3 \alpha_i \mathbf{V}^i(t_0 + 1) = \lambda \mathbf{X}(t_0). \quad (57)$$

Equation (57) can be written in matrix form as:

$$\mathbf{M}\mathbf{X}(t_0) = \lambda \mathbf{X}(t_0). \quad (58)$$

Where the i^{th} column of the monodromy \mathbf{M} is equal to $\mathbf{V}^i(t_0 + 1)$. For equation (58) to have a non-zero solution of $\mathbf{X}(t_0)$, the following equation should be satisfied:

$$|\mathbf{M} - \lambda\mathbf{I}| = 0. \quad (59)$$

Where $||$ denotes the determinant of a matrix. The determination of the stability of the oscillation becomes an eigenvalue problem of the matrix, \mathbf{M} . If the maximum modulus of the eigenvalues is greater than 1, the oscillations are unstable, otherwise the oscillations are stable.

5. EXAMPLE RESULTS

5.1 Water Shell and Water Host Liquid

5.1.1 Fictitious membrane

Consider an air bubble oscillating in water, driven by acoustic pressure of frequency $f = 2.5 \text{ MHz}$. The initial inner and outer radius of the bubble are $R_{10} = 1.2 \mu\text{m}$, $R_{20} = 1.7 \mu\text{m}$. It is noted that according to eq.(50), the excitation frequency is smaller than the natural frequency of the system, since the natural frequency of the single bubble is of 6.9 MHz for mode $n=2$ and the natural frequency will be higher for higher modes. The equations shown in Section 4.4 are solved for different values of the driving pressure, P_a , and the modulus of the resulting eigenvalues are shown in Figure 3 for the $n = 2, 3$, and 4 surface modes. When the eigenvalues are all real, there are three values of the modulus of the eigenvalues. When two of the eigenvalues are complex, their moduli are equal resulting only in only two values of the modulus for 3 eigenvalues. When the amplitude of the driving pressure exceeds $P_a = 0.155 \text{ MPa}$, an eigenvalue of modulus larger than 1 occurs, which indicates that the oscillation becomes unstable.

Figure 4 shows examples of the magnitudes versus normalized time of the a_n (inner shell radius) and b_n (outer shell radius) perturbations for a stable oscillation when the driving pressure is $P_a=0.1\text{Mpa}$ for mode $n=2$. Figure 4a starts from $(a_n, \dot{a}_n, b_n) = (1, 0, 0)$ (i.e. initial perturbation of the inner shell surface) and Figure 4b starts from $(a_n, \dot{a}_n, b_n) = (0, 0, 1)$ (i.e. initial perturbation of the outer shell surface). In both cases, the amplitude of the deformation of the outer surface oscillates with a constant magnitude, while the amplitude of the deformation of the inner surface stays the same or decays to 0 so that the oscillations are stable.

For a higher magnitude of the driving pressure $P_a=0.2\text{Mpa}$ resulting in unstable behavior, the magnitudes of the perturbations are shown in Figure 5. With the initial conditions $(a_n, \dot{a}_n, b_n) = (1, 0, 0)$, (i.e. initial perturbation of the inner shell surface), as shown in the Figure 5(a), the perturbations on both surfaces keep growing from cycle to cycle and deviations from the spherical shape are unstable. However, starting from $(a_n, \dot{a}_n, b_n) = (0, 0, 1)$, (i.e. initial perturbation of the outer shell surface), s shown in the Figure 5(b), the perturbations are see in the right side of the figure to be more stable. The inner surface remains unperturbed, while the outer surface oscillates with a constant amplitude.

It can be proven that when the liquids in the inner and outer domain are the same, one of the eigenvalues is always equal 1.

5.1.2 Presence of a membrane

In the above pure water case, $\rho_1^* = \rho_2^*$, $\mu_1 = \mu_2$ and $\gamma_2 = 0$. Suppose there was a membrane on the outer surface, then we would have $\rho_1^* = \rho_2^*$, $\mu_1 = \mu_2$ and $\gamma_2 \neq 0$. The maximum and minimum eigenvalues with mode $n=2$ of this kind of problems are shown in Figure 6(a) and (b) respectively for different surface tension $\gamma_2 = \gamma_1/100$, $\gamma_1/10$,

$\gamma_1/15$, and $\gamma_1/2$, and are compared with the case of pure water. The figure shows that for small pressure amplitudes ($P_a < 0.04 \text{ MPa}$), the membrane stabilizes the oscillations as the maximum eigenvalues are decreased. This effect is stronger and covers a larger range of excitation pressures for smaller surface tensions.

Another interesting case is when the viscosity in the outer domain is different than that of the shell liquid. The maximum and minimum eigenvalues with mode $n=2$ of this kind of problems are shown in Figure 7 (a) and (b) respectively for different viscosity. The figure shows that by increasing the viscosity in the outer domain, the maximum eigenvalues are decreased for the smaller amplitude P_a , which indicates the oscillations are stabilized. The opposite is true when the outer domain viscosity is lower than that of the shell, while the densities are the same.

5.2 TRIACETIN-SHELLED BUBBLE

For a triacetin-shelled bubble, the highest moduli of the eigenvalues for modes $n=1$ to $n=7$ are shown in Figure 8 for $f = 2.5 \text{ MHz}$ when the shell thickness is $0.5 \mu\text{m}$ and for $R_{10} = 1.2 \mu\text{m}$ and $R_{20} = 1.7 \mu\text{m}$. $R_{10} = 1.2 \mu\text{m}$, $R_{20} = 1.7 \mu\text{m}$. For the triacetin-shelled bubble case, the excitation frequency is also smaller than the natural frequency of the system according to eq. (48). The natural frequency of the triacetin-shelled bubble is of 14.2 MHz for mode $n=2$. The non-dimensional parameters are $R_{e1} = 0.26$, $R_{e2} = 7.23$, $W_{e1} = 3.84$, $W_{e2} = 0.51$, $d_0/R_0 = 0.29$, and $\rho_1/\rho_2 = 1.1$. In the figure the pressures are normalized by $\rho_2 R_{20}^2 f^2$. It can be seen that for normalized pressures of amplitude higher than 75, the largest eigenvalues appear at mode $n=4$, which indicates that $n=4$ is the most unstable mode and the bubble will probably break up into 4 smaller bubbles under this condition. For lower pressures, the most unstable modes are $n=5$ or $n=6$.

To further illustrate when the unstable growth is due to harmonic or to subharmonic resonance, the three real eigenvalues for modes $n=1$ and $n=2$ are shown in Figure 9(a) and (b) respectively. It is seen that the perturbation becomes unstable when the non-dimensional pressure is larger than 80. It is known that when the minimum of the real part of the eigenvalues of the monodromy matrix is below -1, subharmonic resonance occurs whereas harmonic resonance prevails when the maximum real part of an eigenvalue becomes larger than one. Figure 10 shows examples of a growing perturbation for mode $n=1$ and $n=2$ at non-dimensional pressure $\rho_2 R_{20}^2 f^2 = 83$ ($f=2.5\text{MHz}$, $P_a=1.5\text{MPa}$) which will lead to a breakup. The $n=1$ case shows that the perturbation grows unstable at a subharmonic resonance, i.e. the oscillation frequency is smaller than the excitation frequency, while the $n=2$ case shows a harmonic resonance, i.e. the oscillation frequency is equal or larger than the excitation frequency.

The bubble shapes following instability and right prior to breakup are shown in Figure 11 for $n=1,2,3,4$ respectively. The validity of the approach is obviously violated by then. For mode $n=1$, the liquid in the shell layer moves from an side of the layer to the other leaving one side very thin. This is what we observed also in the 3D simulations with large perturbations.¹⁵ The two interfaces become eccentric and a jet initiates on the inner interface while the very thin layer on the other side nears breaking.

For a triacetin-shelled bubble, the liquid in the shell layer is heavier than the surrounding liquid with the density ratio of 1.1. Figure 12 shows that if the inner layer liquid was lighter than the surrounding liquid, the bubble would become more stable as the eigenvalues become smaller when the density ratio is reduced.

To investigate the effect of the viscosity, we calculate the eigenvalues of the oscillation with $R_{e1} = 2.23, R_{e2} = 0.26$ so that the inner layer liquid is less viscous than the outer layer liquid which is opposite to the triacetin-shelled bubble. All other non-dimensional parameters are kept

the same. The eigenvalues for $n=2$ are shown in Figure 13. In this case, the bubbles are more unstable. Furthermore, as shown in Figure 14, the most unstable mode is $n=1$ compared to the most unstable mode $n=4\sim 6$ in Figure 8. Thus the bubble will form a jet on one end and break up on the other end.

6. CONCLUSIONS

The stability of the spherical oscillations of thick-shelled microbubbles or contrast agents were examined using a perturbation theory with harmonic nonspherical small perturbations and solving an eigenvalue problem. The thick-shelled microbubble dynamic equations were derived for the spherical and axisymmetric non-spherical modes. The fastest growing modes were identified by observing the eigenvalues with the largest magnitude. Limits for stability for varying insonification pressure amplitudes were obtained. For a triacetin bubble, where the viscosity in the inner layer is higher than the surrounding liquid, $n=1$ is the most stable mode while for a bubble with less viscous shell, $n=1$ is the most unstable mode.

ACKNOWLEDGMENTS

This work was supported by the National Institute of Biomedical Imaging and Bioengineering under SBIR Phase I and Phase II program.

REFERENCES

1. A. Raisinghani, and A. N. Demaria, "Physical principles of microbubble ultrasound contrast agents," *The American Journal of Cardiology*, **90**, 10A, 3J-7J (2002).

2. R. J. Price, D. M. Skyba, S. Kaul, and T. C. Skalak, "Delivery of colloidal particles and red blood cells to tissue through microvessel ruptures created by targeted microbubble destruction with ultrasound," *Circulation*, 98, 1264-1267 (1998).
3. M. Ward, J. R. Wu and J. F. Chiu, "Ultrasound-induced cell lysis and sonoporation enhanced by contrast agents," *J. Acoust. Soc. Am.* 105, 2951-2957 (1999).
4. P. N. Burns and H. Becher H. *Handbook of Contrast Echocardiography*. Frankfurt: Springer Verlag (2000).
5. J. A. Rooney, "Hemolysis near an ultrasonically pulsating bubble," *Science* **169**, 869-871 (1970).
6. D. L. Miller, R. A. Gies, and W. B. Chrisler, "Ultrasonically induced hemolysis at high cell and gas body concentration in a thin-disc exposure chamber," *Ultrasound in Med. & Boil.* **23**, 625-633 (1997).
7. D. L. Miller, "A Review of the ultrasonic bioeffects of microsonation, gas-body activation, and related cavitation-like phenomena," *Ultrasound in Med. & Biol.* **13**, 443-470 (1987).
8. D. Dalecki, S. Z. Child, C. H. Raeman, C. Xing, S. Gracewski, and E. L. Carstensen, "Bioeffects of positive and negative acoustic pressures in pulsed ultrasound," *Ultrasound in Med. & Biol.* **26**, 1327-1332 (2000).
9. E. Unger, T. P. McCreery, R. Sweitzer, V. Caldwell, and Y. Wu, "Acoustically active lipospheres containing paclitaxel: A new therapeutic ultrasound contrast agent," *Invest Radio*, **12**, 886-892 (1998).
10. P. P. Chang, W. S. Chen, P. D. Mourad, S. L. Poliachik, and L. A. Crum, "Thresholds for inertial cavitation in albumin suspensions under pulsed ultrasound conditions," *IEEE Trans Ultrason. Freq. Control.* **48**, 161-170 (2001).

11. W. S. Chen, T. J. Matula, A. A. Brayman, and L. A. Crum, "A comparison of the fragmentation thresholds and inertial cavitation doses of different ultrasound contrast agents," *J. Acoust. Soc. Am.* **113** (1), 643-651 (2003).
12. A. Prosperetti "Viscous effects on perturbed spherical flows" *Quarterly of Applied Mathematics*, **34**, 339-352 (1977).
13. J.E. Chomas, P.A. Dayton, J. S. Allen, K. Morgan and K. W. Ferrara, "Mechanisms of contrast agent destruction," *IEEE Transactions on Ultrasonics, Ferroelectrics, and Frequency Control*, **48**, 232-248 (2001).
14. E. Coddington and N. Levinson, *Theory of ordinary differential equations*, McGraw-Hill, New York, (1955).
15. C.-T. Hsiao, X. Lu, and G. L. Chahine, "Three-dimensional modeling of the dynamics of therapeutic ultrasound contrast agent," *Ultrasound in Med. & Biol.* **36** (12), 2065-2079 (2010).

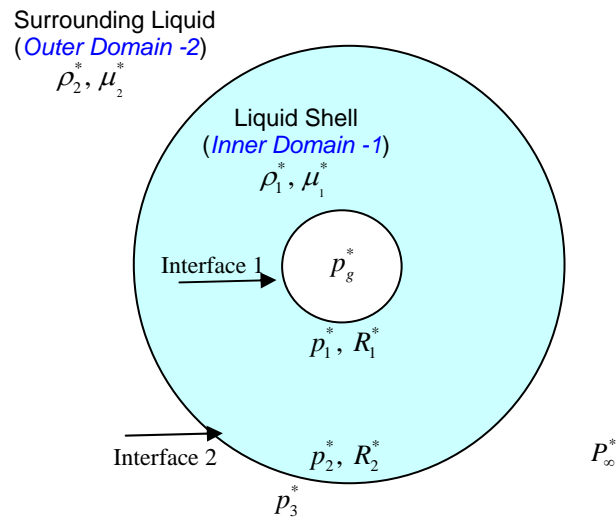


Figure 1. Sketch of the domain for the 1-D spherical thick-shell bubble model.

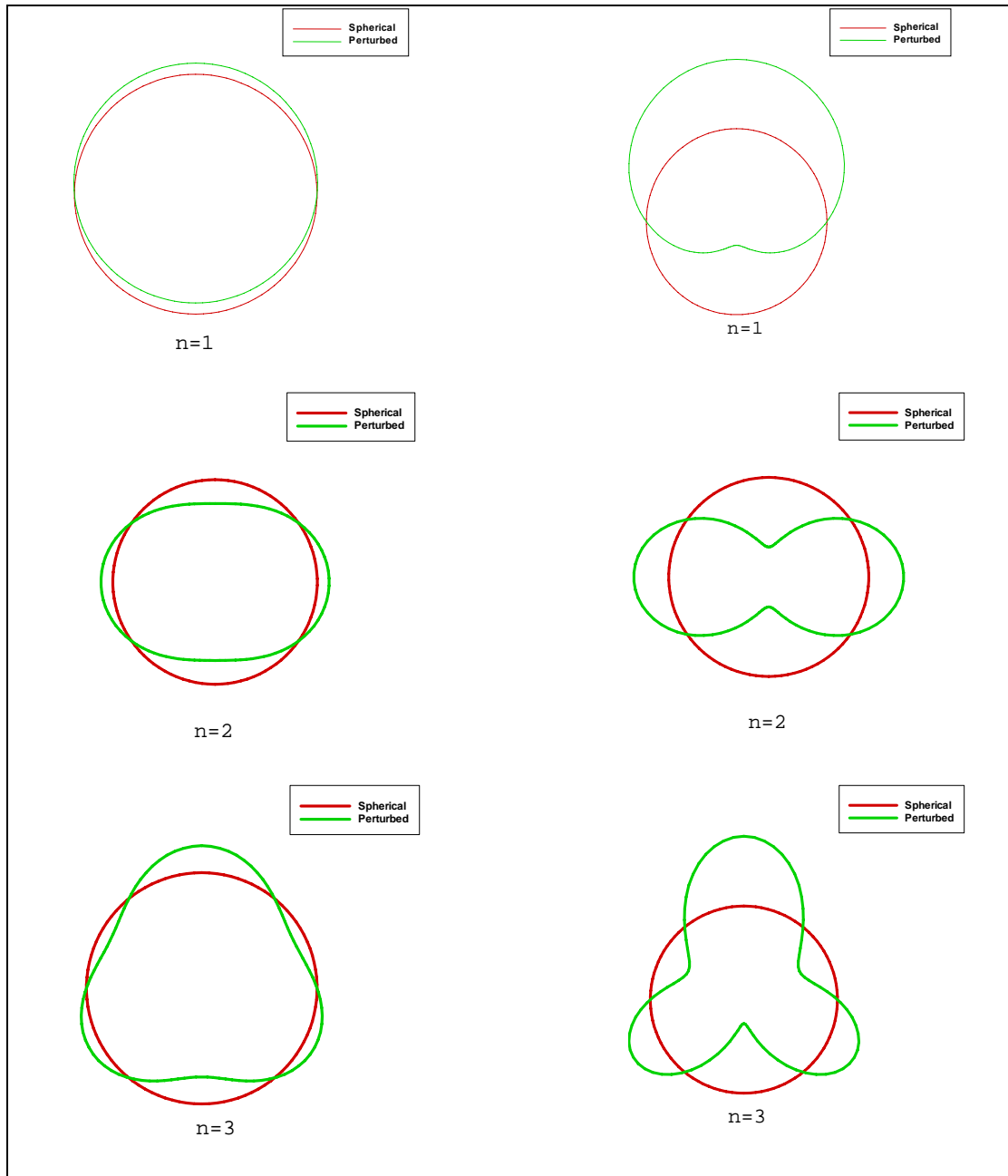


Figure 2. Illustration of the microbubble shape with the existence (small perturbation -left) and growth of perturbations (right) beyond validity of the asymptotic expansions approach for various orders 1 to

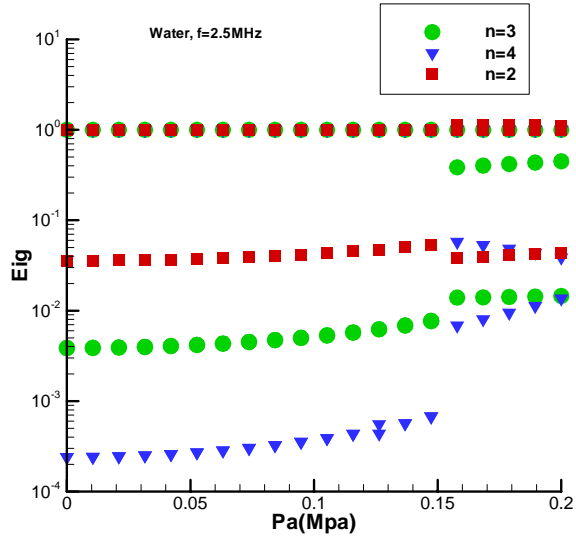


Figure 3. Moduli of the eigenvalues for bubble oscillating in water. Driving acoustic pressure of frequency $f=2.5\text{MHz}$. The initial inner and outer radius of the bubble are

$$R_{10} = 1.2\mu\text{m} \text{ and } R_{20} = 1.7\mu\text{m}.$$

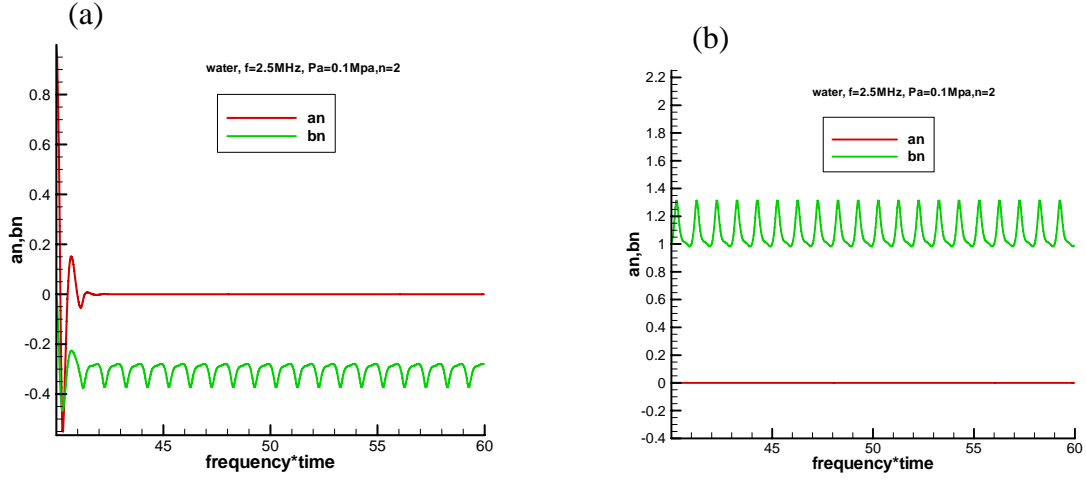


Figure 4. Stable case of a bubble oscillating in water. Variations of a_n (inner shell radius perturbation) and b_n (outer shell radius perturbation) when the driving pressure was $P_a = 0.1 \text{ Mpa}$ and the mode number is $n=2$. (a) Perturbation starts from $(a_n, \dot{a}_n, b_n) = (1, 0, 0)$ and (b) starts from $(a_n, \dot{a}_n, b_n) = (0, 0, 1)$. The initial inner and outer radius of the bubble are $R_{10} = 1.2 \mu\text{m}$ and $R_{20} = 1.7 \mu\text{m}$.

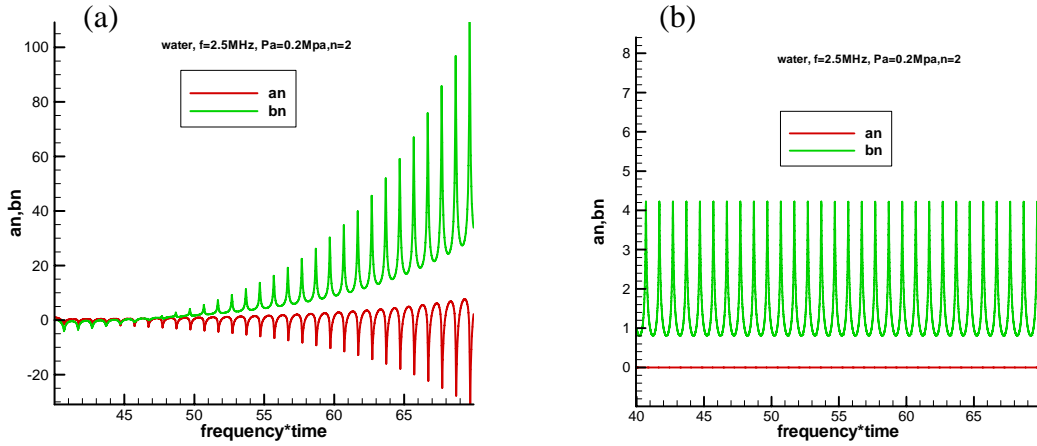


Figure 5. Unstable case of a bubble oscillating in water. Variations of a_n (inner shell radius perturbation) and b_n (outer shell radius perturbation) when the driving pressure was $P_a = 0.2 \text{ Mpa}$ and the mode number is $n=2$. (a) Perturbation starts from $(a_n, \dot{a}_n, b_n) = (1, 0, 0)$ and (b) starts from $(a_n, \dot{a}_n, b_n) = (0, 0, 1)$. The initial inner and outer radius of the bubble are $R_{10} = 1.2 \mu\text{m}$ and $R_{20} = 1.7 \mu\text{m}$.

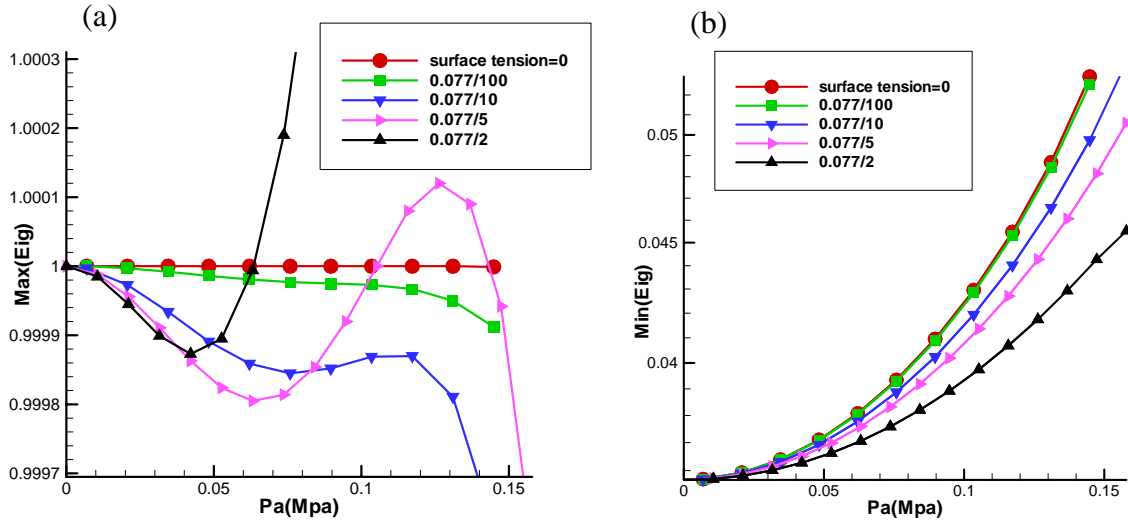


Figure 6. Influence of the excitation pressure on the eigenvalues of the perturbation for a water shell in water host liquid with a membrane between the two. (a) maximum modulus of eigenvalue (b) minimum modulus of eigenvalue for $\rho_1^* = \rho_2^*$, $\mu_1 = \mu_2$ and $\gamma_2 = 0$, $\gamma_1/100$, $\gamma_1/10$, $\gamma_1/15$, and $\gamma_1/2$.

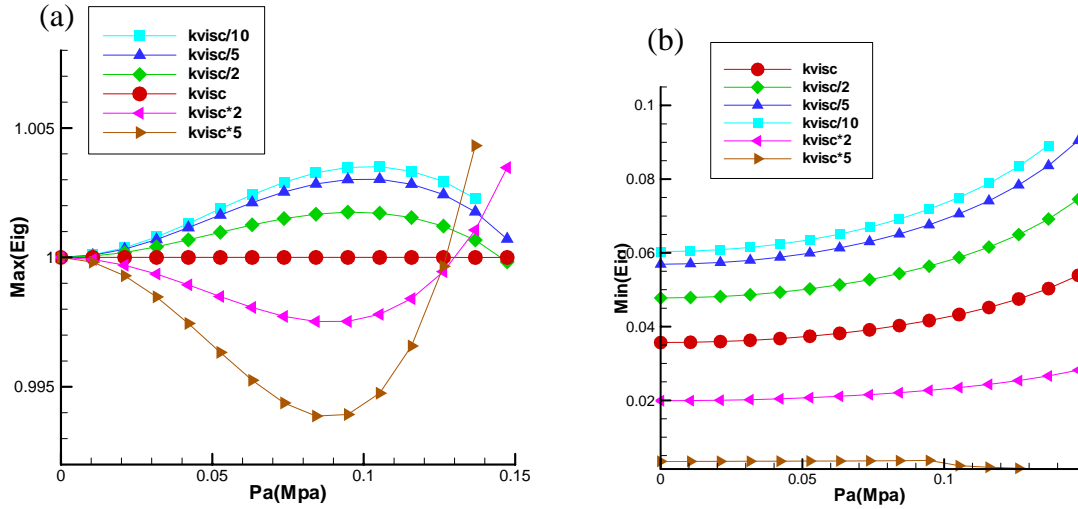


Figure 7. Influence of the excitation pressure on the eigenvalues of the perturbation for a water shell in a host liquid with various viscosities. (a) maximum modulus of eigenvalue (b) minimum modulus of eigenvalue for $\rho_1^* = \rho_2^*$, $\gamma_2 = 0$ and $\mu_1 = \mu_2/10$, $\mu_2/5$, $\mu_2/2$, μ_2 , $2\mu_2$, and $5\mu_2$.

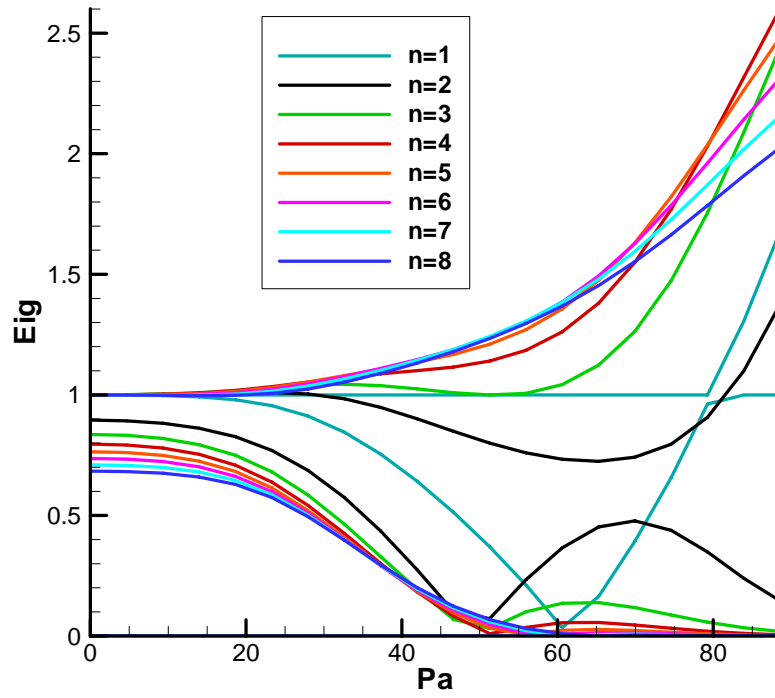


Figure 8. Modulus of eigenvalues of the oscillation of triacetin-shelled bubble driven by pressure at

$f=2.5\text{MHz}$, initial shell thickness= $0.5\ \mu\text{m}$. The pressures are normalized by $\rho_2 R_{20}^2 f^2$.

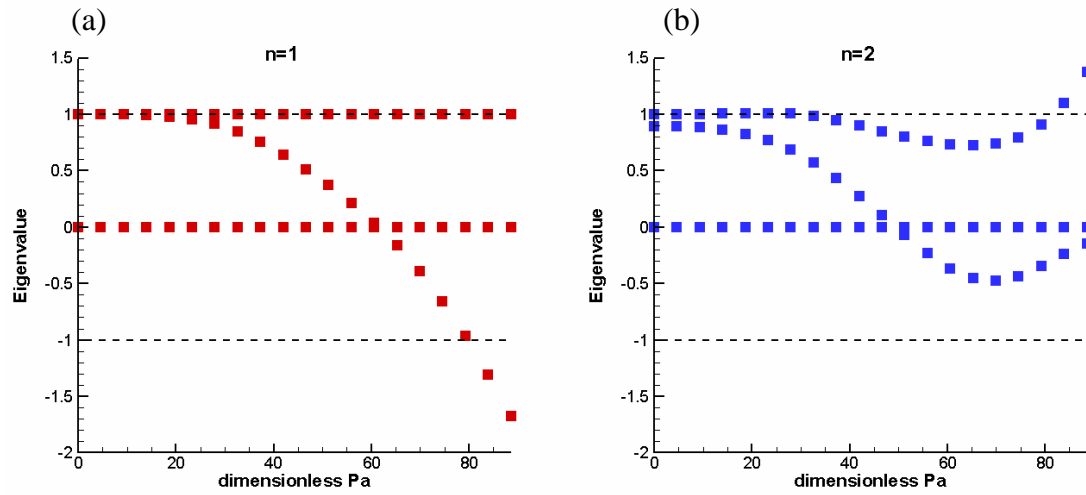


Figure 9. Real eigenvalues of the oscillation of triacetin-shelled bubble driven by pressure at $f=2.5\text{MHz}$, initial shell thickness= $0.5\ \mu\text{m}$ (a) mode $n=1$ (b) mode $n=2$. The pressures are normalized by

$$\rho_2 R_{20}^2 f^2.$$

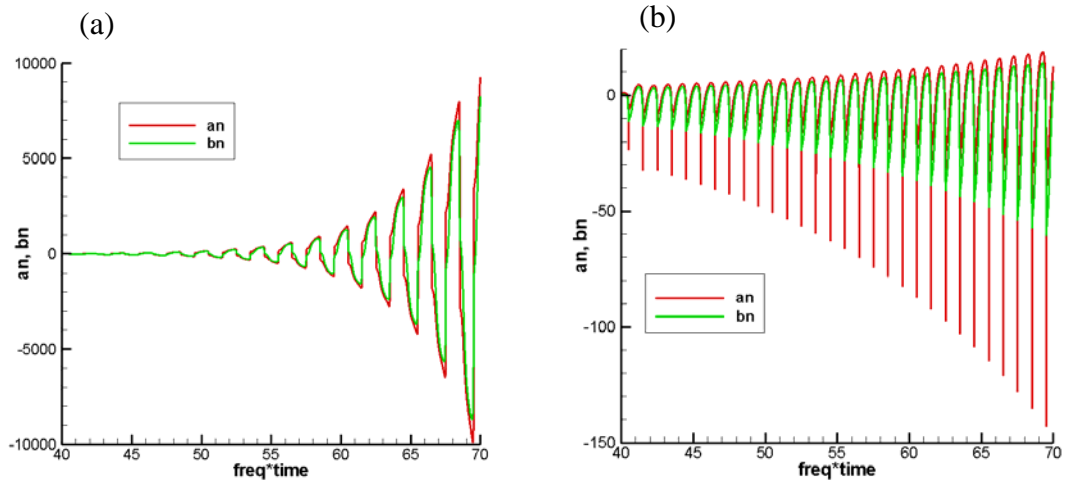


Figure 10. Growing perturbations for an oscillating triacetin-shelled bubble. (a) mode $n=1$, (b) mode $n=2$ for $f=2.5\text{MHz}$, $P_a=1.5\text{Mpa}$, $n=2$

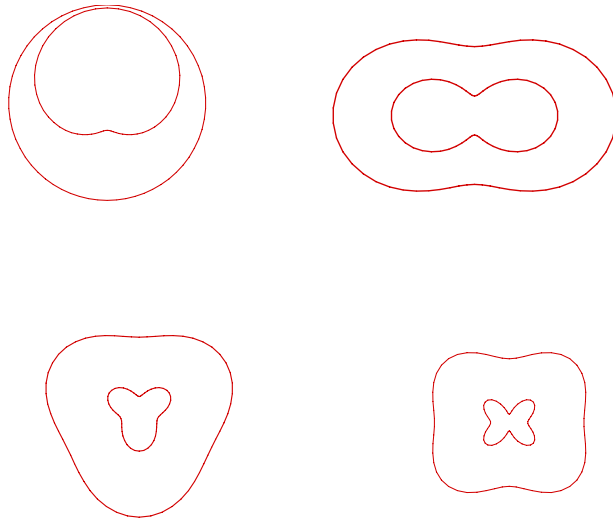


Figure 11. Bubble shapes before breaking up with perturbation mode $n=1,2,3,4$ respectively.

$f=2.5\text{MHz}$, $Pa=1.5\text{Mpa}$

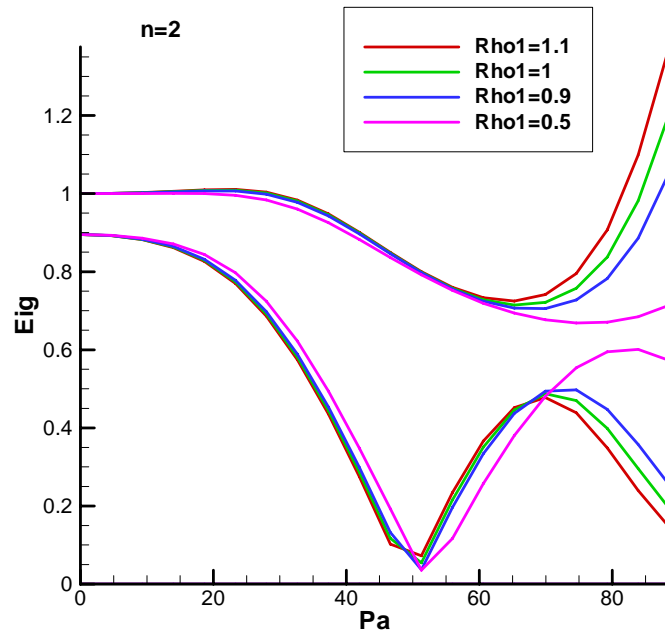


Figure 12. Effect of the density ratio on the stability of mode 2. $f=2.5\text{MHz}$, $R_{e1}=0.26$, $R_{e2}=2.23$.

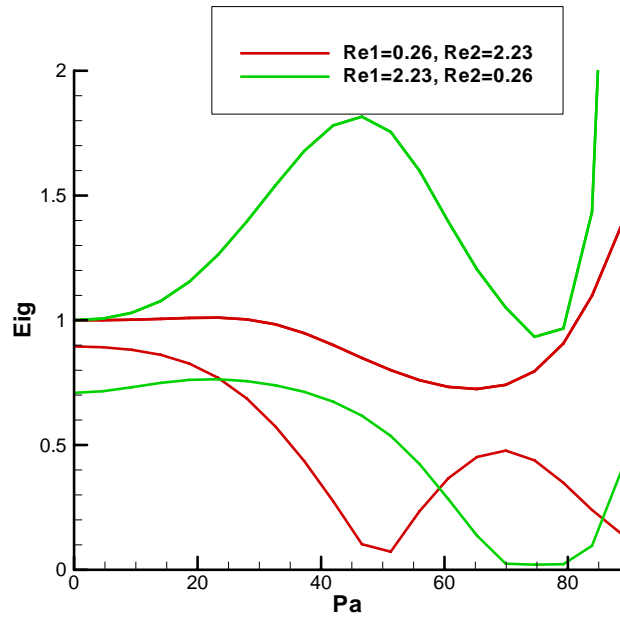


Figure 13. Effect of viscosities on the eigenvalues for $n=2$, $f=2.5\text{MHz}$, density ratio=1.1.

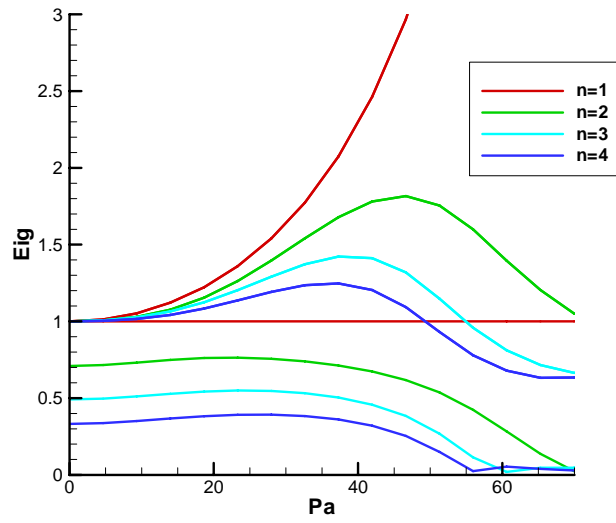


Figure 14. Effect of reducing the viscosity of the liquid in the shell layer $R_{e1}=2.23, R_{e2}=0.26, f=2.5\text{MHz}$, density ratio=1.1.